

Recent Experiments on the STOR-M Tokamak*

C. Xiao¹, T. Onchi¹, Y. Liu¹, S. Elgriv¹, M. Dreval^{1,2}, D. McColl¹, T. Asai³,
and A. Hirose¹

¹Department of Physics and Engineering Physics, University of Saskatchewan,
Saskatoon, Saskatchewan S7N 5E2, Canada
(chijin.xiao@usask.ca)

²Institute of Plasma Physics NSC KIPT, Kharkov, Ukraine

³Department of Physics, Nihon University, Tokyo 101-8308, Japan

Abstract

Recent experiments on the STOR-M tokamak have been focused on basic tokamak physics and technology development for controlled thermonuclear fusion research. Active control of the magnetohydrodynamic (MHD) instabilities has been achieved by helical resonant magnetic perturbations (RMPs). Improved confinement has been induced by gas puffing during ohmic discharges. Modification of toroidal flow velocities by a tangentially injected compact torus (CT) plasmoid to the STOR-M discharge has been observed.

1. Experimental Setup

The Tokamak is the most promising configuration for thermonuclear fusion reactors based on magnetic confinement. STOR-M is a small research tokamak in the Plasma Physics Laboratory at the University of Saskatchewan [1]. The shape of the tokamak plasma resembles a donut. The major and minor radii of the STOR-M tokamak are 46 cm and 12 cm respectively. The toroidal magnetic field is 0.7 T and discharge current 20 kA for a typical discharge. Hydrogen gas is admitted through a gas valve and the plasma density can be controlled by additional preprogrammed gas puffing. The STOR-M is equipped with various diagnostic tools including a 4 mm interferometer for density measurement, a spectrometer for monitoring H_{α} and impurity radiation intensities, a soft x-ray (SXR) imaging camera for measurement of SXR emissivity profiles in the plasma [2], an ion Doppler spectrometer (IDS) for plasma flow velocity measurement, and several Mirnov coil arrays to monitor MHD instabilities.

The University of Saskatchewan Compact Torus Injector (USCTI) is a coaxial gun for forming and accelerating a high density plasmoid confined by magnetic field [3]. CTs accelerated to high velocities were proposed by Perkins *et al.* [4] and Parks [5] and demonstrated by Raman [6] as a means for direct fuelling of the core of tokamak fusion reactors. The inner and outer radii of the acceleration electrodes in USCTI are 1.8 cm and 5 cm respectively. Typically, USCTI produces CTs with a density of $5 \times 10^{16} \text{ cm}^{-3}$ and velocity of 150-250 km/s. The particle inventory in CT is 0.5 μg , approximate 50% of that in a STOR-M plasma. Considering the toroidal flow velocity of tokamak plasma in the range of several kilometres per second, the momentum in an USCTI CT is

* This work was sponsored by the Canada Research Chair Program and Natural Sciences and Engineering Research Council of Canada.

approximately an order of magnitude higher than that in a STOR-M discharge. The unique feature of the CT injection experiments on STOR-M is the tangential injection configuration for investigation of momentum injection by CT injection. Figure 1 shows the sketch of the top view of the STOR-M tokamak with USCTI installed for tangential injection experiments. The insert shows the CT magnetic signals detected in the formation region ($z = 0$ cm) and three other locations along the acceleration electrode. The delay of the signals can be used to measure the CT velocity through time-of-flight approach.

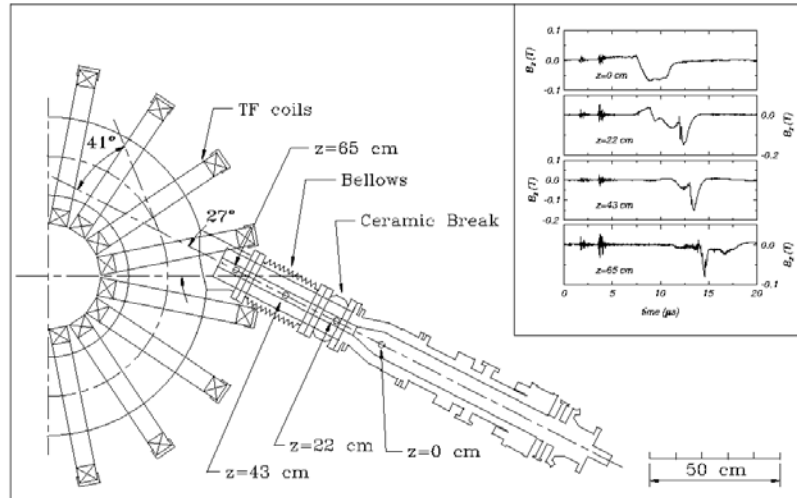


Figure 1 Diagram of the STOR-M tokamak and the USCTI injector for tangential CT injection experiments.

In a tokamak discharge, MHD instabilities driven by current density gradient tend to grow on specific rational magnetic surfaces and form magnetic island along closed helical structures. The modes of the MHD instability structure are characterized by poloidal (goes around the circumference of the cross-section of the torus) mode number m and toroidal (goes around the circumference of the torus) mode number n . The helical structure goes around the toroidal direction m times and poloidal direction n times before closing on itself. In Fig. 2, the black line depicts the $m = 2, n = 1$ mode. The blue and red lines are two sets of external $m = 2$ and $n = 1$ helical coils offset by 90° in the poloidal direction. The two coils are connected in such a way that a power supply drives currents through the two coils with equal magnitude and opposite directions as shown by the arrows on the coils. The magnetic field created by this set of helical coils has the ability to control the targeted MHD (2,1) mode through resonant interactions [7].

In the following Sections, results of the following three experiments will be presented: (a) control of MHD instabilities by helical RMP, (b) improved confinement induced by gas puffing, and (c) momentum injection by tangential CT injection. For each experiment, the motivation and significance will be described before the results are presented.

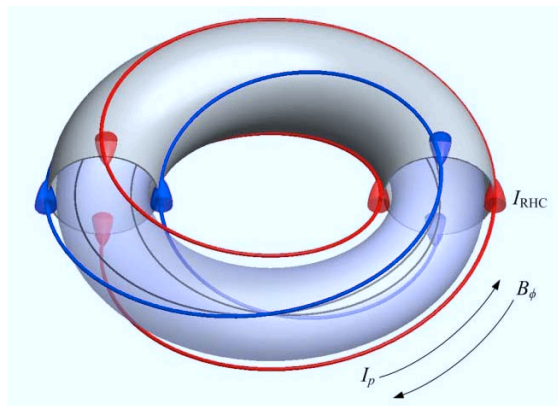


Figure 2 Illustration of the $m = 2$ and $n = 1$ MHD mode (thin black lines) in a tokamak plasma and the corresponding resonant helical coils (thick red and blue lines) used to control the instability.

2. Control of MHD Instabilities through Resonant Magnetic Perturbations

MHD instabilities in a tokamak are global instabilities driven by current density and/or pressure gradients. MHD instabilities not only cause loss of energy and particles in the plasma, but also trigger minor and, in some cases, major disruptions [8]. A particular type of MHD instabilities, known as tearing modes or magnetic islands, grows on certain radial locations with characteristic modes (m, n) discussed in Section 1. The magnetic fields, plasma density and plasma temperature deviate from the equilibrium quantities in the magnetic islands. Rotation of the mode structures will cause fluctuations in the signals detected by the detectors installed on fixed locations. The fluctuations associated with the tearing mode instabilities in tokamaks, such as Mirnov oscillations and sawtooth oscillations, are usually monitored by various diagnostics and analyzed using a number of data processing techniques. Mirnov and sawtooth oscillations do not affect too much the operation of the tokamak, hence can be observed during the normal operation. Under certain circumstances, certain MHD modes are also precursors of major disruptions which cause termination of the tokamak discharge. Sudden quench of the large current may induce intolerable electromagnetic forces on the magnet coils and the support structures. It is important to monitor the MHD instabilities and find the way to suppress them.

In many tokamaks, the major disruptions are likely caused by the interaction of $(2, 1)$ magnetic islands with the limiter or with the edge plasma [9] or by mode coupling between the growing $(2, 1)$ island with $(1, 1)$ mode [10] or with $(3, 2)$ mode [11]. Some early experiments have showed that the growth of $(2, 1)$ mode could be influenced by applying magnetic field perturbations produced by an $(l = 2, n = 1)$ resonant helical coil (RHC) installed outside the tokamak vacuum chamber [12]. The DC currents applied to RHC is usually small (typically 1% to 4% of the plasma current). It has been observed that RMP can effectively reduce the width of magnetic islands and hence suppress the Mirnov oscillations [13]. Plasma stabilization has also been achieved by AC currents with its amplitude regulated by a mode-locking feedback system. Other common applications of RMPs involve error field corrections, edge localized modes (ELMs) control, and runaway electrons suppression.

The influence of RMP plasma parameters has been experimentally examined on STOR-M. During the discharge #246961, a helical current pulse of about 5 ms was applied when the MHD oscillations

are large. The discharge parameters shown in Fig. 3(a) are, from the top, plasma current I_p , loop voltage V_l , horizontal plasma position ΔH , edge safety factor $q(a)$, H_α radiation intensity, hard x-ray (HXR) emission, SXR emission and Mirnov fluctuations. In this discharge ($I_p = 25.5$ kA, $V_l = 2.5$ V, $q(a) = 3.7$), the I_{RMP} pulse was applied at 12 ms after the plasma ramp-up for a duration of 5 ms. The current in RHCs is about 600 A (2.4% of total plasma current). Clear reduction in HXR emission level has been observed approximately 0.6 ms after applying I_{RHC} . The plasma column is shifted by 5 mm outwards. The main effect of I_{RMP} on the discharge is the significant suppression in MHD fluctuation signal and increased SXR emission from the plasma core. Figure 3(b) shows the expanded waveforms of I_{RMP} , Mirnov fluctuation signals, and the wavelet spectrum of Mirnov signal. The suppression of Mirnov oscillations does not occur immediately after the I_{RMP} is applied. After 0.5 ms, the amplitude of MHD oscillations is strongly suppressed between 12.5 ms and 17 ms. During the I_{RMP} pulse, a sudden reduction in MHD amplitude and frequency between 12.5 ms and 17 ms can be also seen on the wavelet spectrum. The MHD frequency is reduced from 26 kHz to 15 kHz. After I_{RMP} is turned off, the MHD oscillations amplitude and frequencies return to the nominal values.

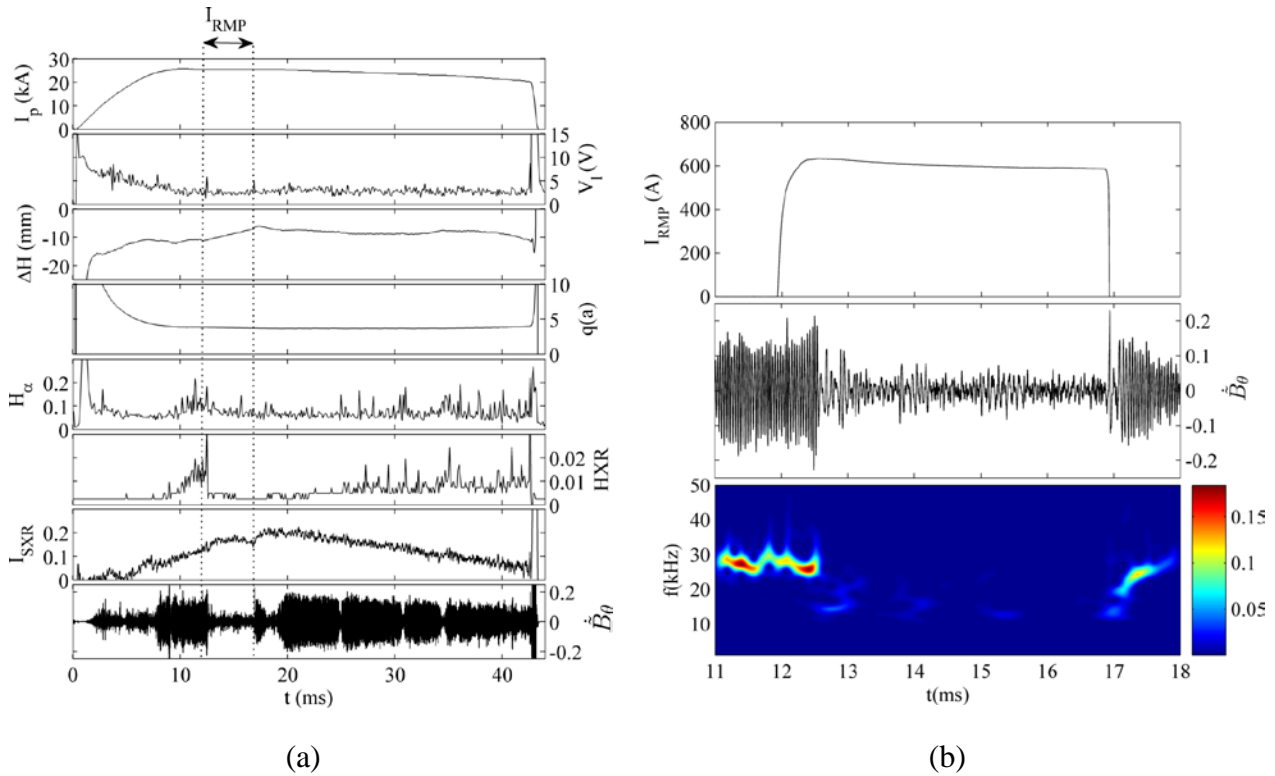


Figure 3 Effects of helical RMP on plasma parameters during the STOR-M discharge #246961. The resonant field was applied at 12 ms for about 5 ms during the plasma current plateau.

The spatial structure and temporal evolution of MHD modes can be analyzed using the singular value decomposition (SVD) algorithm [14] using poloidal Mirnov coil arrays. Figures 4(a), (b) and (c) show the spatial structure (panels on the top) and the temporal features (panels at the bottom) of poloidal MHD modes before (11-12ms), during (13-16ms) and after (17-18ms) the I_{RMP} pulse are applied.

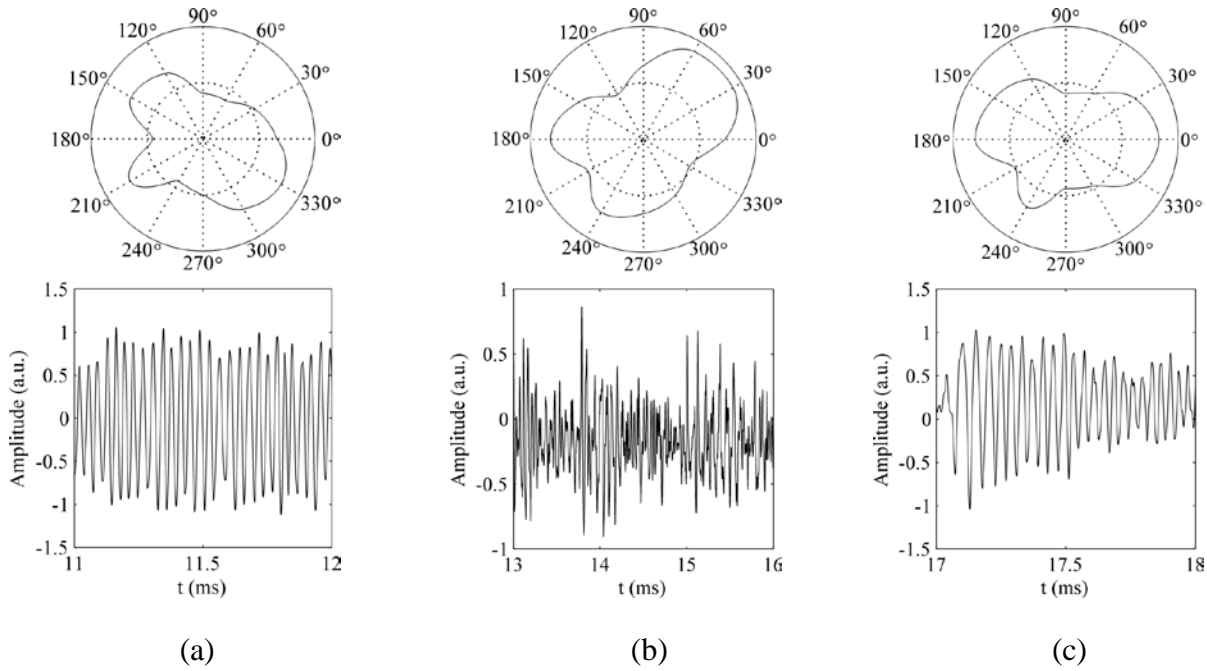


Figure 4 Spatial structure and temporal evolutions of dominant poloidal MHD modes (a) before (b) during and (c) after applying I_{RMP} as extracted by SVD.

The spatial structure of main $m=2$ is distorted by $m=3$ and $m=4$ modes as shown in Fig. 4. The toroidal mode number corresponds to $n=1$ in this discharge, which is the typical case for most of STOR-M discharges. The coupled MHD spatial harmonics can be calculated by performing a spatial Fourier analysis on the distorted poloidal distribution pattern. Figure 5(a) shows the relative decomposed poloidal mode spectra by spatial Fourier analysis for three time durations: before (11-12ms, blue), during (13-16ms, green) and after (17-18ms, brown) the I_{RMP} pulse are applied. Before firing I_{RMP} , the coupled modes, $m=2$ mode ($\sim 60\%$) and $m=4$ mode ($\sim 26\%$) dominate. During the MHD suppression phase (13-16ms), the relative amplitude of the $m=2$ mode is reduced to 54% while the $m=3$ mode increases to 31%. After turning off I_{RMP} , the $m=2$ mode grows again as a dominant mode (80%), while the $m=3$ mode reduces to 16%. Apparently I_{RMP} does not have a strong effect on $m=1$ mode since it maintains the same relative amplitude in the three cases. Note that the plots are percentage amplitudes normalized for signals within each time window.

The magnitudes of harmonics from $m=1$ to $m=4$ modes can also be obtained using the signals from 12 Mirnov coils distributed in the poloidal angles. The spatial Fourier series decomposes the sine and cosine components of each mode at any fixed time. The analysis was performed on the time segment 11-18 ms (1 ms before and after applying I_{RMP}). The mode magnitudes are plotted in Fig. 5(b). The $m=2$ (blue) and $m=4$ (green) modes have the highest magnitude before firing the I_{RMP} pulse. There is a slight reduction in mode magnitudes of $m=1$ and $m=3$ after applying the helical current. In contrast, the $m=2$ magnitude responds almost immediately to RMP and increases by 43% before it drops suddenly by 90% at 12.5 ms. The $m=4$ fluctuation amplitude is also reduced significantly by 86%. The suppression lasts for about 4.5 ms until $t=17$ ms when the modes start

oscillating at their original amplitudes prior to applying I_{RMP} , with $m = 2$ being the dominant mode again.

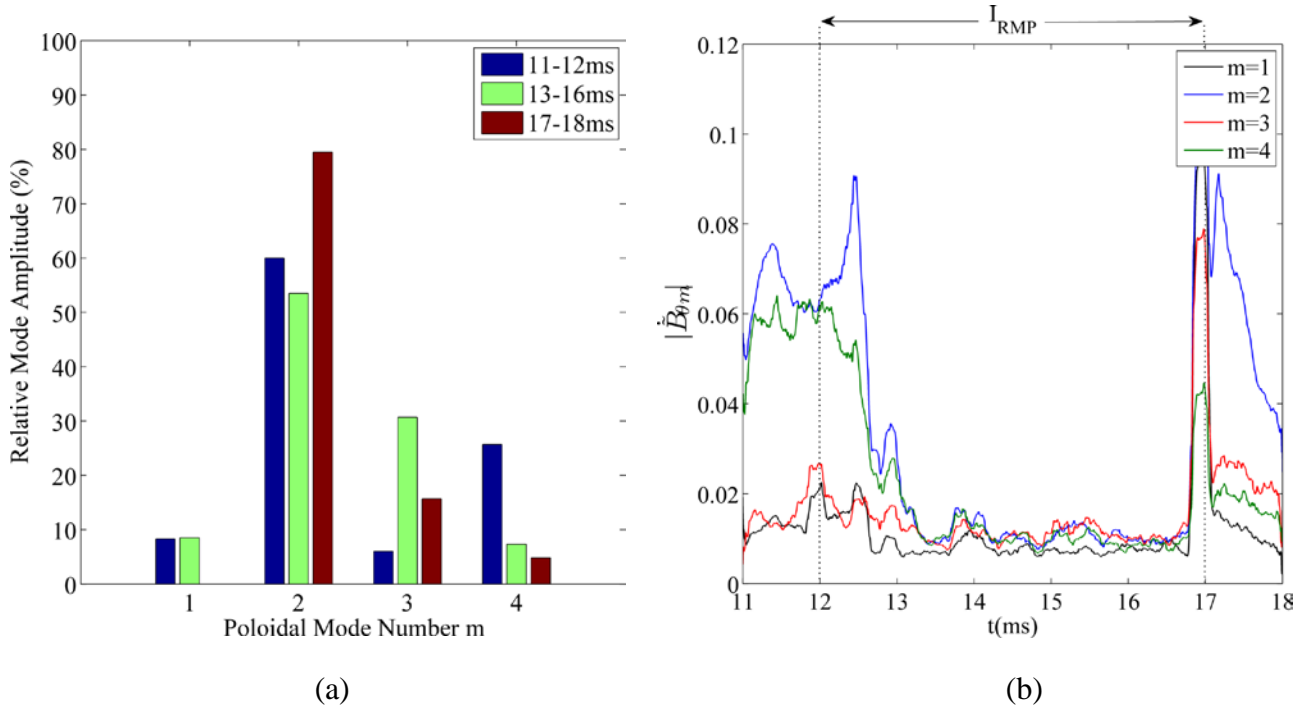


Figure 5 (a) Spatial Fourier analysis of spatial structures before, during, and after applying I_{RHC} . (b) Mode magnitudes for MHD modes up to $m = 4$ around the time of firing I_{RHC} .

3. Improved Confinement Induced by Gas Puffing

One of the major obstacles for realization of fusion reactors is the anomalous transport about two orders of magnitudes above the level predicted by classical theory which accounts only for Coulomb collisions between charged particles. Improved confinement mode opens a route towards economically viable fusion reactors. Since the discovery of the improved confinement mode (H-mode) in the neutral-beam heated ASDEX tokamak in 1982 [15], ohmic H-modes have also been found in many tokamaks without auxiliary heating. Taylor *et al.* found that a shear of the poloidal flow due the $\mathbf{E} \times \mathbf{B}$ drift in the edge region is responsible for reducing the turbulence induced anomalous transport and triggering H-mode [16]. The poloidal flow shear is also intimately related to the steepening of pressure profile at the edge plasma. The edge transport barrier (ETB) has been formed on STOR-M by externally applied electric field through electrode or limiter biasing, short current pulse through edge heating due to skin effects, compact torus injection (CT) due to interaction between CT and tokamak plasmas.

In fact, many plasma parameters can affect the poloidal flow shear which is the key for ETB by reducing the sizes of turbulence eddies. The poloidal flow velocity based on force balance of the tokamak plasma can be expressed by

$$v_{\theta} = -\frac{E_r}{B_t} - \frac{T_i}{qn_i B_t} \frac{dn_i}{dr} - \frac{1}{qB_t} \frac{dT_i}{dr} + \frac{B_{\theta}}{B_t} v_t \quad (1)$$

where v_g is the poloidal velocity, v_t the toroidal velocity, B_g the poloidal magnetic field, B_t the toroidal magnetic field, E_r the radial electric field, T_i the ion temperature, n_i the ion density, and q the ion charge. This equation clearly shows that modification of one or more parameters may lead to ETB and trigger H-mode. In the Alcator C-Mod tokamak, formation and evolution of the edge barrier and the accompanied enhanced confinement regime have been reported [17]. The neutrals can enter the edge dynamics through inter-related particle, momentum, and energy balance. More recently, H-mode like discharges have also been induced by preprogrammed puffing of gas during STOR-M discharges.

Figure 6 (a) shows waveforms of a STOR-M discharge. The steady flow of the working gas is hydrogen. During the flat-top of the STOR-M current, a sharp hydrogen gas is puffed into the discharge at $t = 17$ ms. On the left hand side of Fig. 6(a) the following traces are shown (from top): discharge current, loop voltage, horizontal position displacement, ion saturation current (a measure of plasma density) at $r = 13.5$ cm, line average electron density measured by interferometer through a central chord, and the gas puffing control voltage pulses. The traces on the right hand side of Fig. 6(a) are (from top): toroidal Mach number measured by a Gundestrup probe at $r = 13.5$ cm (positive value indicates co-current flow direction), floating potential (DC component) measured at $r = 13.5$ cm, root-mean-square (RMS) level of the floating potential fluctuations at $r = 13.5$ cm, the RMS level of the magnetic fluctuations measured externally, soft x-ray (SXR) radiation level from the central region, and the H_α radiation level. The traces clearly show transition from L-mode to H-mode after second gas puffing pulse. The main features the H-mode-like phase include: (a) reduction in the loop voltage without change in discharge current, a sign of increased Spitzer temperature, (b) increase in the line average electron density and the edge electron density, (c) toroidal flow breaking, (d) negative auto-biasing of plasma potential, (e) suppression of both electrical and magnetic fluctuation levels, (f) significant increase of SXR radiation level, and (g) decrease in the H_α radiation level.

Figure 6 (b) shows the improvement of several key parameters during the H-mode-like discharge phase triggered by gas puffing. The traces shown are (from top): poloidal beta, global energy confinement time, and the Spitzer temperature. A brief temperature increase corresponds to the brief loop voltage reduction or the reduction in plasma resistivity which is inversely proportional to $T_e^{3/2}$. The poloidal beta value is ratio of the plasma thermal energy density to the poloidal magnetic field energy density. the poloidal magnetic field energy density is approximately constant since the plasma current is almost constant. The poloidal beta value in this case is proportional to the product of the density and temperature. The relatively long phase of the improved poloidal beta value (more than doubled) is mainly due to the density increase and the small initial peak is due to the temperature increase. The global energy confinement time (more than quadrupled) is proportional to the thermal energy in the plasma and inversely proportional to heating power which can be expressed by $P = I_p \cdot V_L$ for the ohmic STOR-M discharge. The more pronounced initial peak in the energy confinement is due to the small initial peak in the poloidal beta compounded by the short dip in the loop voltage.

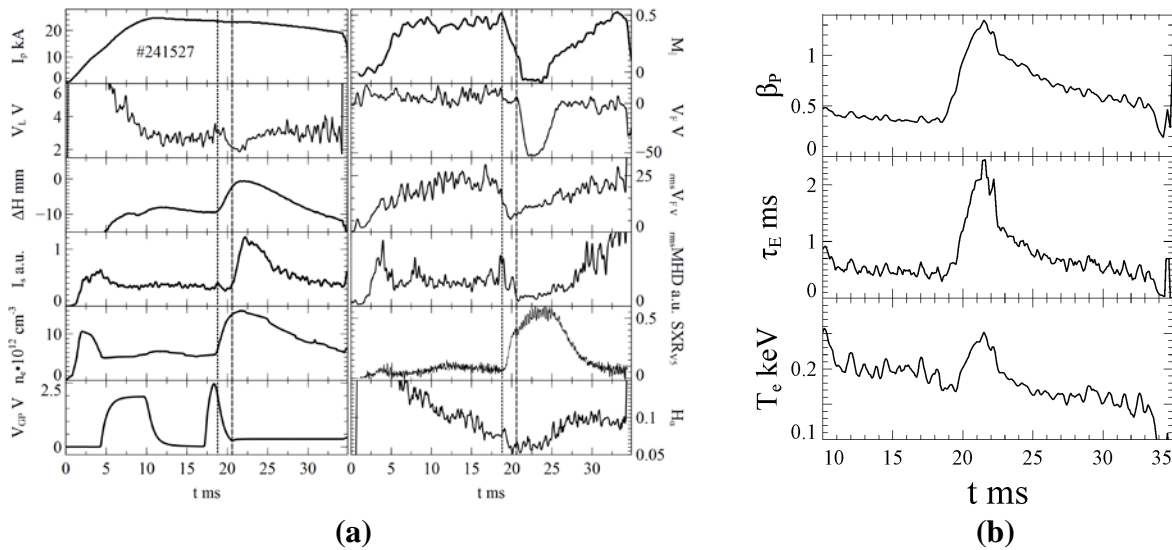


Figure 6 (a) Waveforms of plasma current, loop voltage, horizontal plasma position, averaged ion saturation current(13.5cm), line-average electron density, additional gas puffing pulses, parallel Mach number (13.5 cm), floating potential (13.5cm), RMS of floating potential fluctuations, RMS of magnetic probe fluctuations, SXR emission from the central region, H_{α} radiation level. (b) Waveforms poloidal beta, energy confinement time, and average electron temperature.

4. Momentum Injection by Tangential CT Injection

As indicated in Equation (1), the toroidal plasma flow is one of the factors determining the poloidal flow. The shear of the poloidal flow is thought to be responsible for breaking up the turbulent eddies in plasmas and for reducing turbulence induced radial transport. Toroidal flow plays also roles for stabilizing resistive wall modes. Development of techniques to drive and control toroidal flow is important for fusion research.

The main purpose of compact torus (CT) injection is for fuelling of fusion reactors. A high velocity CT carries also large momentum. In STOR-M, the CT injector is installed tangential to the tokamak torus, as shown in Fig. 1, and thus tangential CT injection has the possibility to drive toroidal flow by momentum injection in the counter-clockwise direction for the configuration shown in Fig. 1.

On STOR-M, toroidal flow can be measured by using Gundestrup probe in the plasma edge. Non-intrusive IDS measurement [18] extends flow measurement to the core plasma if certain impurity ion emission lines are bright enough for detection. In STOR-M tokamak, the following 3 impurity emission lines are used: a C_{III} line (464.7 nm) mainly from the radial location near $r = 7$ cm, O_V line (650.0 nm) at $r = 4$ cm, and C_{VI} line (529.0 nm) near the center of the tokamak.

Figure 7 shows the flow measurements for three similar shots with CT injected at $t = 20$ ms. The plasma current was in the counter-clockwise direction (top view) and toroidal magnetic field in clockwise direction as shown in Fig. 2. In Fig. 7, the positive flow points in the counter-clockwise direction or co-current direction. The thick dashed lines indicate the trend of the flow velocities for the baseline discharges without CT injection. It can be seen that the outer-most impurity C_{III} rotates in the co-current direction, the same direction as the plasma flow direction at the edge plasma measured with

the Gundestrup probe (see M_{\square} trace in Fig. 6(a)). The initial O_V line in the intermediate radial location starts at almost zero flow velocity. Finally, the C_{VI} line near the plasma core rotates in the anti-current direction. Under those discharge conditions, all three flow velocities at different radial locations decreases towards anti-current direction at about similar rate, indicating that the toroidal velocity shear of those impurity ions does not change over time. The observation shows that the impurity ions, and likely also the bulk plasmas, rotate in the co-current direction at the plasma edge and anti-current direction in the core plasma.

From about 0.7 ms after CT injection, all flow velocities increase towards the co-current direction, the same direction as the CT injection direction, suggesting momentum input from CT to tokamak discharge. It can be seen that the toroidal flow increases by the largest (smallest) amount for the ion at the inner-most (outer-most) radial locations and last the longest (shortest) period of time. This observation suggests that the transfer of the CT momentum occurred mainly in the core region.

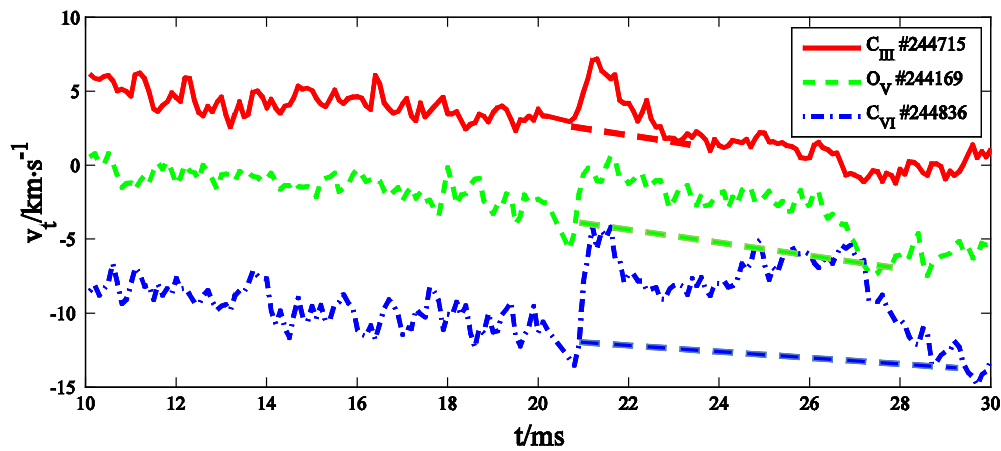


Figure 7. The toroidal flow velocity of C_{III} line (464.7 nm, $r \square 7$ cm), O_V line (650.0 nm, $r \square 4$ cm) and C_{VI} line (529.0 nm, $r \square 0$ cm) during CT injection experiments. The CT is injected at 20 ms. The thick dashed lines indicate the trend of the flow velocities for the baseline discharges without CT injection.

Although CT injection also induces H-mode-like confinement, the modification of the flow velocity may not be attributed the H-mode itself. For example, in the H-mode-like phase induced by gas puffing discussed in Section 3, the plasma flow at the edge speeds up in the anti-current direction (see again M_{\square} trace in Fig. 6(a)), opposite to the change of flow velocity induced by CT injection for the C_{III} ion near the edge. Although the main plasma and the impurity ion velocity may differ in magnitude, they should agree with each other qualitatively.

In order to confirm the plasma flow directions in relation to discharge current direction in the STOR-M tokamak and to study the effects of CT injection on the toroidal plasma flow, plans have been made to perform CT injection experiments with tokamak plasma current reversed to the clockwise direction. The IDS measurements depicted in Figure 8 shows that the impurity velocity also reversed when the tokamak discharge current direction is reversed, suggesting that the plasma current direction in the plasma is the key parameter determining the velocities of impurity ion, and most likely also velocities

of the bulk plasma. After a technical problem is corrected for the USCTI injector, effects of CT injection on the tokamak discharge with reversed plasma current direction will be investigated in the near future.

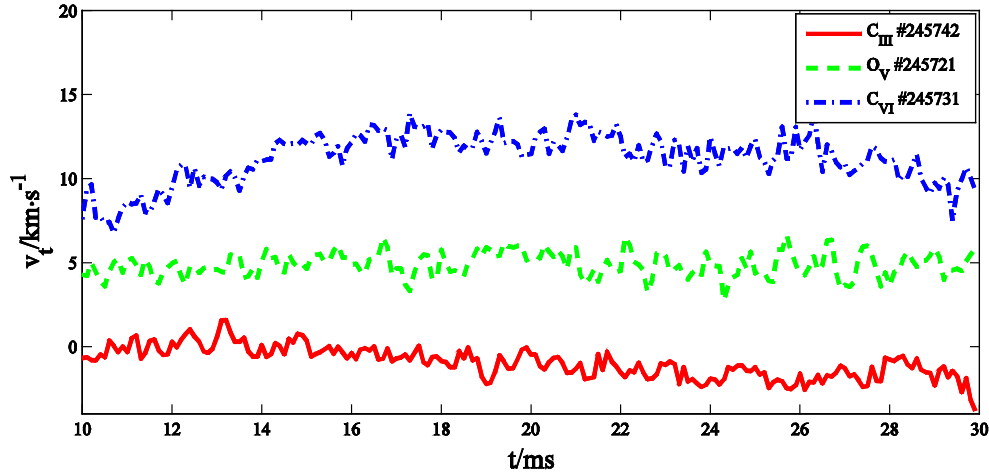


Figure 8. The toroidal flow velocity of C_{III} , O_V and C_{VI} impurities for a discharge with reversed tokamak discharge current direction. No CT was injected during this discharge.

5. Conclusion

Several recent experiments on the STOR-M tokamak have been successfully carried out. Resonant magnetic perturbations (RMPs) using ($l=2, n=1$) helical coils have effectively suppressed the ($m=2, n=1$) MHD mode. Before application of RMP, strong $m=2$ and $m=4$ poloidal modes dominate. During RMP, both $m=2$ and $m=4$ are suppressed by more than 85%. After RMP, the Mirnov oscillations return to high levels. After a fast gas puffing pulse, an H-mode-like discharge phase is induced in STOR-M. The main features of the H-mode-like phase include increase of electron density and temperature, increase in SXR radiation intensity, decrease in H_α radiation level, suppression of floating potential and magnetic fluctuations, and increase in global energy confinement time. Momentum transfer from a tangentially injected CT to STOR-M discharges has been observed. Before CT injection, the impurity in the outer region of the plasma always rotates in the co-current direction and the impurity in the inner region of plasma always rotates in the counter-current direction. After CT injection, the flow velocity of impurity ions all increase towards CT injection direction. The flow velocity increases the most and lasts the longest in the core region of the plasma. The ability to control the MHD instabilities and the plasma flow has important implications in the future reactor design by reducing heat load bursts on the chamber wall and by reducing the requirements on installation accuracy of the magnet coils. Improved confinement operation mode will also reduce the operation cost of fusion reactors and thus make the reactor more economical.

6. References

1. A. Hirose, C. Xiao, O. Mitarai, J. Morelli, H.M. Skarsgard, "STOR-M Tokamak Design and Instrumentation", Physics in Canada, Vol 62, 2006, pp. 111-120.

2. C. Xiao, T. Niu, J.E. Morelli, C. Paz-Soldan, M. Dreval, S. Elgriw, A. Pant, D. Rohraff, D. Trembach and A. Hirose, “Design and initial operation of multichord soft x-ray detection arrays on the STOR-M tokamak”, *Rev. Sci. Instrum.*, Vol. 79, 2008, pp. 10E926-1-3.
3. C. Xiao, S. Sen and A. Hirose, “Improved confinement induced by tangential injection of compact torus into the Saskatchewan Torus-Modified (STOR-M) tokamak”, *Phys. Plasmas*, Vol. 11, 2004, pp. 4041-4049.
4. L.H. Perkins, S.K. Ho and J.H. Hammer, “Deep penetration fuelling of reactor-grade tokamak plasmas with accelerated compact toroids”, *Nucl. Fusion*, Vol. 28, 1988, p. 1365.
5. P.B. Parks, “Refueling Tokamaks by Injection of Compact Toroids”, *Phys. Rev. Lett.*, Vol. 61, 1988, p. 1364.
6. R. Raman, F. Martin, B. Quirion, *et al.*, “Experimental Demonstration of Nondisruptive, Central Fueling of a Tokamak by Compact Toroid Injection”, *Phys. Rev. Lett.*, Vol 73, 1994, pp. 3101-3104.
7. S. Elgriw, D. Liu, T. Asai, A. Hirose and C. Xiao, “Control of magnetic islands in the STOR-M tokamak using resonant helical fields”, *Nucl. Fusion*, Vol. 51, 2011, p. 113008.
8. A. Sykes and J. A. Wesson, “Major disruptions in tokamaks”, *Phys. Rev. Lett.*, Vol. 44, 1980, pp. 1215-1218.
9. D. E. Roberts, J.A.M. De Villiers, J.D. Fletcher, J.R. O'Mahony and A. Joel, “Major disruptions of low aspect ratio tokamak plasmas caused by thermal instability”, *Nucl. Fusion*, Vol. 26, 1986, p. 785.
10. P. V. Savrukhin, E. S. Lyadina, D. A. Martynov, D. A. Kislov and V. I. Poznyak, “Coupling of internal m=1 and m=2 modes at density limit disruptions in the T-10 tokamak”, *Nucl. Fusion*, Vol. 34, 1994, pp. 317-336.
11. B. V. Waddell, B. Carreras, H. R. Hicks, J. A. Holmes and D. K. Lee D. “Direct ion heating through MHD relaxation”, *Phys. Rev. Lett.*, Vol 41, 1978, pp. 1386-1390.
12. F. Karger, H. Wobig, S. Corti *et al.*, “Influence of resonant helical fields on tokamak discharges”, 1975 in *Plasma Physics and Controlled Nuclear Fusion Energy Research, Proceedings of 5th IAEA Int. Conf. Tokyo*, Vol. 1, 1974, p. 207-215.
13. J. J. Ellis, A. A. Howling, A. W. Morris and D. C. Robinson, “The influence of resonant helical fields on tokamak confinement”, 1984 *IAEA Proc. 10th Int. Conf. on Plasma Physics and Controlled Nuclear Fusion*, Vol. 1, pp. 363-373.
14. C. Nardone, “Multichannel fluctuation data analysis by the singular value decomposition method”, *Plasma Phys. Control. Fusion*, Vol. 34, 1992, pp. 1447-1465.
15. F. Wagner, G. Becker, K. Behringer, *et al.*, “Regime of improved confinement and high beta in neutral-beam-heated divertor discharges of the ASDEX tokamak”, *Phys. Rev. Lett.*, Vol. 49, 1982, pp. 1408-1412.
16. R. J. Taylor, M. L. Brown, B. D. Fried, H. Grote, J. R. Liberati, G. J. Morales, and P. Pribyl, “H-mode behavior induced by cross-field currents in a tokamak”, *Phys. Rev. Lett.*, Vol. 63, 1989, pp. 2365-2368.

17. R. L. Boivin, J. A. Goetz, A. E. Hubbard, *et al.*, “Effects of neutral particles on edge dynamics in Alcator C-Mod plasmas”, *Phys. Plasmas*, Vol. 7, 2000, pp. 1919-1926.
18. J. H. F. Severo, I. C. Nascimento, Yu. K. Kuznetov, *et al.*, “Plasma rotation measurement in small tokamaks using an optical spectrometer and a single photomultiplier as detector”, *Rev. Sci. Instrum.*, Vol. 78, 2007, pp. 043509-1-5.